# B-DNA's $B_I \rightarrow B_{II}$ Conformer Substate Dynamics Is Coupled with Water Migration

**Rudolf H. Winger, Klaus R. Liedl,* Simon Rüdisser, Arthur Pichler, Andreas Hallbrucker, and Erwin Mayer**

*Institute of General, Inorganic and Theoretical Chemistry, University of Innsbruck, Innrain 52a, A-6020 Innsbruck, Austria*

*Received: July 17, 1998; In Final Form: August 18, 1998*

The *Eco*RI DNA dodecamer d(CGCGAATTCGCG)$_2$ is investigated by state-of-the-art molecular dynamics simulations. The $B_I \rightarrow B_{II}$ transition is shown to be a consequence of destacking processes of adjacent base pairs and is coupled with migration of water from ionic phosphate to the sugar oxygen. Two-thirds of the double-helical base steps temporarily are in the $B_{II}$ substate. The time-averaged $B_I/B_{II}$ population ratio is 9.2, but at a given time, it can be as low as 2.7. Observed changes in the solvation properties closely match recently reported spectroscopic features. The different time scales of all processes involved are discussed with respect to experimental results. Formation of contact ion-pairs is demonstrated to be independent of substate transitions.

## Introduction

The dynamical behavior of B-DNA, especially the interconversion between its conformational substates during complex formation, is thought to play a decisive role for its biological function (e.g., substrate binding)[1,2] and misfunction (e.g., mutation).[3] The major and minor grooves along the helical axis are not only vital for interactions with small ligands like water[4] and drugs[5] but they also play a dominant role in the interaction with proteins[6,7] and other nucleic acid molecules.[8] The importance of the backbone phosphate groups has been shown in numerous investigations.[9−21] The simulation presented herein is investigated with respect to the different conformational substates of the B-form: the $B_I$ and $B_{II}$ states. Their existence was first suggested[22] and shown by X-ray crystallography[23,24] and later inferred from NMR spectroscopy,[25−28] molecular modeling studies,[29] and molecular dynamics (MD) simulations.[30,31] Conformational substates of B-DNA were recently detected by Fourier transform infrared spectroscopy,[32] but it was not clear whether these were the $B_I$ and $B_{II}$ substates seen in single crystal X-ray diffraction studies. For the unambiguous determination of the $B_I$ and $B_{II}$ substates by NMR see Szyperski et al.[33] A recent review by Berman[34] summarizes B-DNA crystallography and $B_I-B_{II}$ characteristics. The two B-form substates are defined by different conformations of the sugar−phosphate backbone (Figure 1).

In the $B_I$-state the corresponding $\epsilon$ and $\zeta$ angles derived from X-ray structures are between 120° to 210° (trans) and 235° to 295° (gauche$^-$), respectively, for $B_{II}$ $\epsilon$ lies between 210° and 300° (gauche$^-$), $\zeta$ between 150° and 210° (trans).[35] Investigations of four decamer X-ray structures[36] resulted in a hypothesis for $B_I-B_{II}$ transitions: Grzeskowiak et al.[36] suggested that unfavorable base stacking interactions induce destacking processes which consequently allow the $B_I-B_{II}$ interconversion. These transitions, especially if both strands are involved, lead to a widening of the minor groove.[36−38]

The sequence investigated here, d(CGCGAATTCGCG)$_2$, is also known as the "*Eco*RI dodecamer" because its central six base pairs are the recognition site for the *Eco*RI endonuclease. This dodecamer duplex was the first oligonucleotide duplex found to be in the B-form of DNA[23,39−45] and subsequently was the target of further crystallographic experiments.[46,47] Additionally, a large number of both experimental and theoretical studies including NMR experiments,[48−50] Raman spectroscopic investigations,[51] and MD simulations[31,49,52−61] was carried out and excellently reviewed by Young et al.[31] In the crystalline form, the *Eco*RI dodecamer displays unsymmetric axis bending at the junctions between AATT and CGCG which, taking into account the symmetry of the sequence, was interpreted to result from crystal packing effects[40,41] and/or the kinetics of crystallization.[23] These suggestions are confirmed by the fact that the slightly modified CGCGAATT$^{Br}$CGCG dodecamer under different conditions crystallizes in a straight conformation.[23] In the X-ray structure of the duplex complexed with the *Eco*RI enzyme, a kink induced by ligand binding is observed.[62,63] NMR experiments[48] and Raman spectra[51] as well as circular dichroism

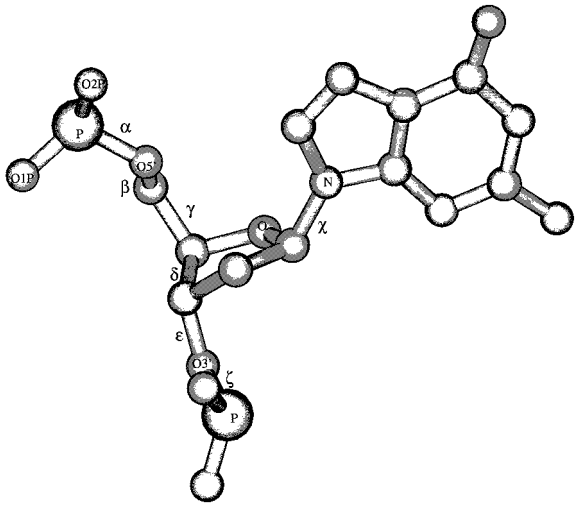


**Figure 1.** Definition of the characteristic DNA backbone torsional angles: The DNA backbone is shown along with one base. The ball-and-stick representation was created using MOLDEN 3.2.[90]

* Corresponding author.

10.1021/jp983005f CCC: $15.00 
Published on Web 10/13/1998

studies[64] suggest a conventional B-form structure in solution. Evidence for conformational substates $B_I$ and $B_{II}$ in the X-ray structure were initially attributed to crystal packing effects.[65−67] Later on, the already mentioned spectroscopic and modeling experiments suggested the existence of these conformational substates in solution and thus in the biologically active form.

## 2. Methods

Molecular dynamics (MD) simulations provide an excellent and unique tool, as the complete elucidation of the DNA's structure in its biologically active form is still difficult by current experimental methods. For reviews of DNA simulations, we refer to von Kitzing,[68] Beveridge et al.,[69,70] and Lousie-May et al.[71] The investigation of dynamics allows insights into time dependent conformational changes. Due to the fast interconversion between conformational substates of DNA, which are assumed to interconvert at physiological temperatures on the nanosecond and sub-nanosecond time scale,[25−28,33,72,73] current simulation techniques allow a detailed investigation.

Although the description of the B-form with older force fields was problematic,[31,56] nowadays MD-simulations are able to provide stable B-form DNA trajectories[31,59,60] due to the better parameterization of the force fields and the inclusion of the long-range interactions, above all the Ewald summation which is implemented in the AMBER program[74] in the form of the so-called particle mesh Ewald method.[75,76] Various investigations stress the significance of MD simulations for the description of DNA: different B-form starting structures converge,[77] starting from B-form and A-form results in the B-form[61,78] and finally the initial ion placement is arbitrary as long as the long range interactions are treated correctly.[31] MD-simulations taking into account those improvements are now successfully applied to nonnatural PNA helices[79] and DNA triplex systems.[80]

**2.1. Computational Details.** To obtain the best possible description, the findings of previous extensive simulations[31,59,81,82] were directly adapted for our simulation protocol. The canonical B-form[83,84] of the DNA oligonucleotide $d(CGCGAATTCGCG)_2$ was used as starting point. Each strand contains 11 $PO_4^-$ anions and is terminated with OH groups. Electroneutrality of the system was achieved by 22 $Na^+$ counterions using the CION-program of the AMBER package. Subsequent solvation of the DNA with TIP3P[85] Monte Carlo water boxes requiring a 12 Å thick solvent shell in all directions resulted in a system of the dimensions $68 \times 45 \times 45$ Å$^3$ containing 3784 water molecules. The corresponding $\Gamma$-value (i.e., water molecules per nucleotide) is about 158. The simulation was carried out using the AMBER 4.1 suite of programs employing the all atom force field[86] for the DNA and counterions.

Minimizations were carried out, starting with 500 steps and harmonic restraints of 25 kcal mol$^{-1}$ Å$^{-2}$ on DNA and counterion positions. During the following five 100-step minimizations the restraints on the counterions were relaxed faster than on the DNA duplex. Finally, 500 steps of unrestrained minimization were carried out. For the equilibration a similar procedure was applied. After heating the constant volume system during 10 ps from 50 to 300 K and keeping the DNA and ion positions constant, the harmonic restraints were reduced throughout the following 25 ps, on the counterions faster than on the oligonucleotide. Finally, a 5 ps unrestrained constant-volume simulation was carried out before the simulation was switched to constant-temperature and constant-pressure MD. The temperature bath coupling was achieved by the Berendsen algorithm.[87]

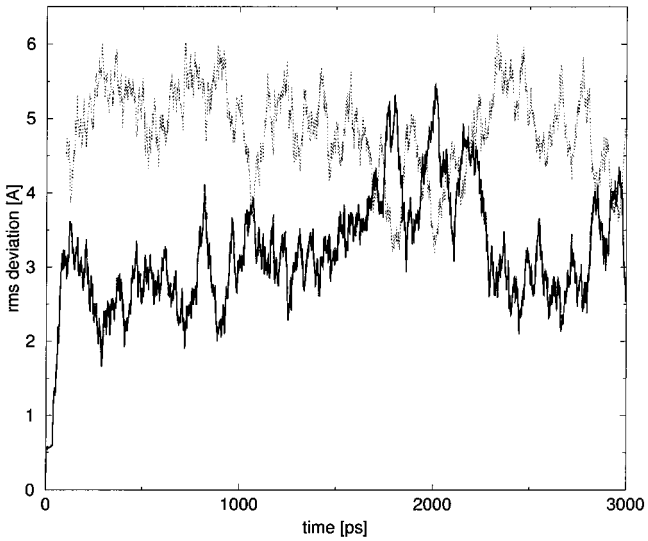


**Figure 2.** Root mean square deviation of the simulated structures with respect to the canonical B-DNA starting structure (bold line) and with respect to canonical A-DNA (dashed line).

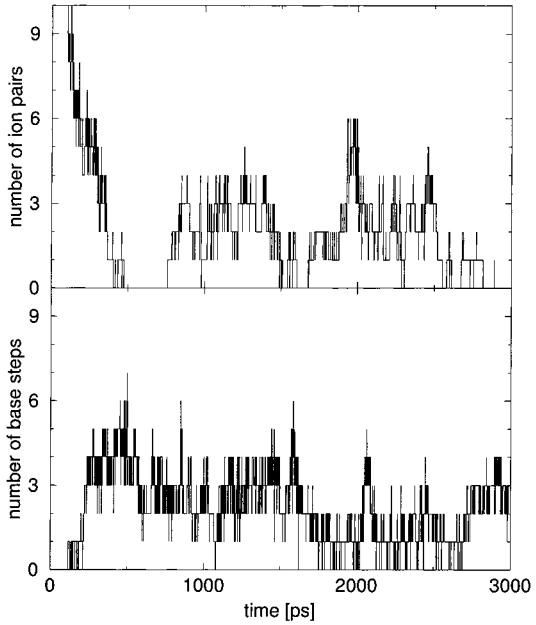


**Figure 3.** Number of ion pairs (top) between the sodium counterions and the ionic phosphate oxygen atoms and the number of base steps in the $B_{II}$ substate (bottom) as a function of time.

General simulation parameters were kept constant during the whole simulation: 2 fs time step, SHAKE constraints of 0.00005 Å on all bonds involving hydrogen atoms, 9 Å nonbonded cutoff, and 0.00001 convergence criterion for the Ewald part of the nonbonded interactions. The structural information was collected every 50 steps (0.1 ps).

## 3. Results

**3.1. General Characteristics.** In order to obtain a reliable thermodynamical ensemble, the starting point for analysis was chosen to be at 1.0 ns. After 1.0 ns of equilibration, the overall structural features represented as the root mean square deviation (rmsd) (Figure 2) were rather constant, and also the ion pair formation processes and the $B_I-B_{II}$ transitions were equilibrated (Figure 3).

The stability of the overall structure in the B-form can easily be seen from the rmsd development, which oscillates around

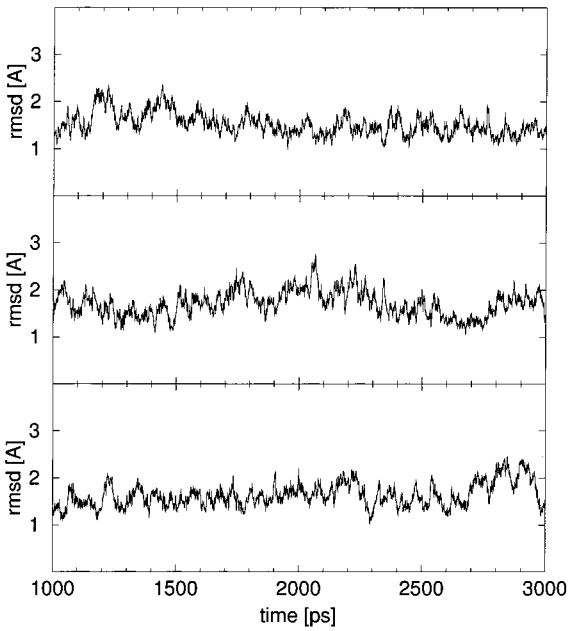


**Figure 4.** Root mean square deviation of the 5′-$(CGCG)_2$ (top), the $(AATT)_2$ (middle), and the terminal $(CGCG)_2$ part (bottom) of the dodecamer duplex with respect to canonical B-DNA.

**TABLE 1: Averages and Standard Deviations of Backbone $\chi$-Angles (1600−2400 ps) and Their Comparison with A- and B-DNA Values Derived from X-ray Structures**

| base number | $\bar{x}$ | $\sigma(\chi)$ | base number | $\bar{x}$ | $\sigma(\chi)$ |
|---|---|---|---|---|---|
| C1 | 247.16 | 36.449 | C13 | 225.70 | 22.796 |
| G2 | 246.79 | 13.983 | G14 | 254.67 | 20.364 |
| C3 | 226.98 | 13.803 | C15 | 232.57 | 16.493 |
| G4 | 245.78 | 12.737 | G16 | 222.71 | 19.032 |
| A5 | 225.06 | 16.012 | A17 | 223.04 | 15.622 |
| A6 | 228.59 | 15.757 | A18 | 226.67 | 15.434 |
| T7 | 231.35 | 14.953 | T19 | 230.79 | 14.313 |
| T8 | 231.18 | 16.260 | T20 | 227.30 | 15.387 |
| C9 | 229.90 | 22.014 | C21 | 228.74 | 15.987 |
| G10 | 237.22 | 17.971 | G22 | 256.26 | 18.351 |
| C11 | 232.48 | 15.023 | C23 | 233.78 | 13.912 |
| G12 | 243.25 | 19.922 | G24 | 249.51 | 25.036 |
| B-form | 241/258[35] | | A-form | 199[35] | |

3.2 Å with respect to the canonical B-form and 4.8 Å with respect to the canonical A-DNA.[83] The slightly increased rmsd around 2000 ps is no indication for B−A transition, as detailed analysis of the rmsd of the CGCG termini and the AATT core with respect to the canonical B-form (Figure 4) revealed no concerted transition.

Investigation of the $\chi$ angles between 1600 and 2400 ps further demonstrate B-type behavior, as shown in Table 1.

The averaged structure from 1.0 to 3.0 ns is shown in Figure 5 along with the canonical B-DNA structure and the X-ray structure of the Drew−Dickerson dodecamer. This averaged structure exhibits close resemblance to both experimental structures. An extensive discussion of the stability of B-DNA using an identical simulation protocol is given by Young et al.[31]

**3.2. B-DNA Substates.** In the course of the simulation the number of phosphate groups in the $B_{II}$ substate ranged from 0 to 6, resulting in a $B_I/B_{II}$ ratio as low as 2.7 (see in Figure 3 at 450, 800, and 1600 ps). The time-averaged number of base steps in the $B_{II}$ state is 2.16 (about 10%, $B_I/B_{II}$ ratio = 9.2). This is in agreement with the dodecamer's X-ray structure, which shows a comparable number of $B_{II}$ states. The important difference lies in the individual base steps involved and their $B_{II}$ occupation as a function of time.

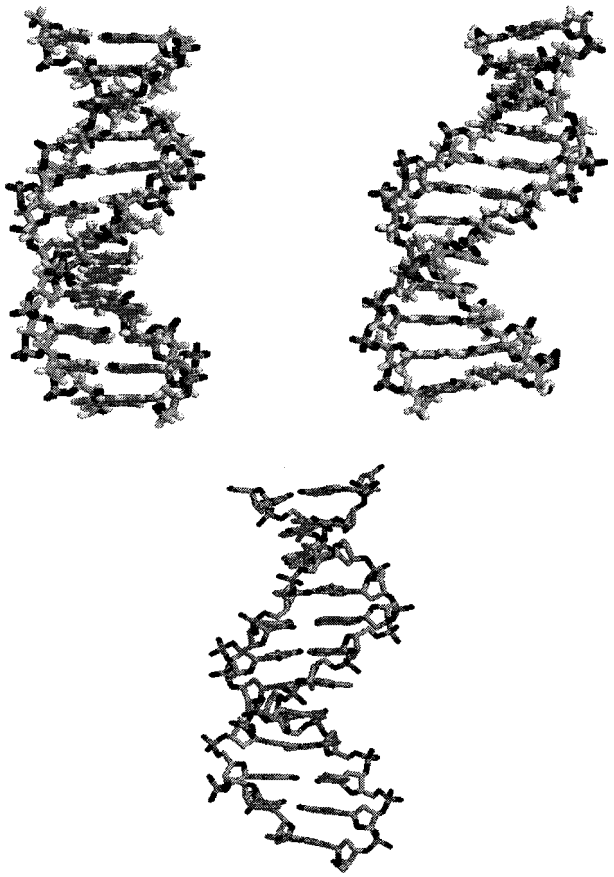

**Figure 5.** Comparison between the canonical B-DNA starting structure (left), the simulation structure averaged from 1000 to 3000 ps (right), and the X-ray structure[47] (bottom).

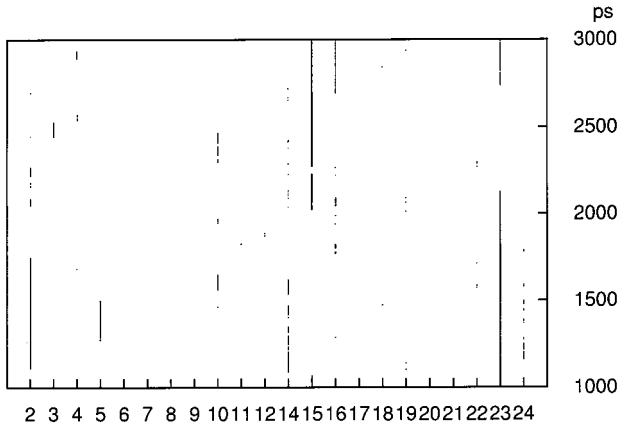


**Figure 6.** Conformational substates as a function of time: The time the respective $\epsilon$-angle of the 22 phosphates is in substate $B_{II}$ is marked by a black line/dot. Enumeration of the interconverted phosphate groups is according to Kopka et al.[45]

The complete set of all $\epsilon$-angles and their conformation as a function of time is depicted in Figure 6 for the 22 phosphates of the dodecamer's 22 base steps.

It is interesting to note that out of the 22 possible base steps 15 show at least once an interconversion to the other B-substate, but only half of them remain in the $B_{II}$ substate for a longer period. The most prominent backbone changes appear in both CGCG-termini of both strands. The major base steps involved are the C1−G2 (phosphate 2), G4−A5 (phosphate 5), C13−G14 (phosphate 14), G14−C15 (phosphate 15), C15−G16 (phosphate 16), and G22−C23 (phosphate 23) steps. Between 300 and 1000 ps the G10−C11 (phosphate 11) step is

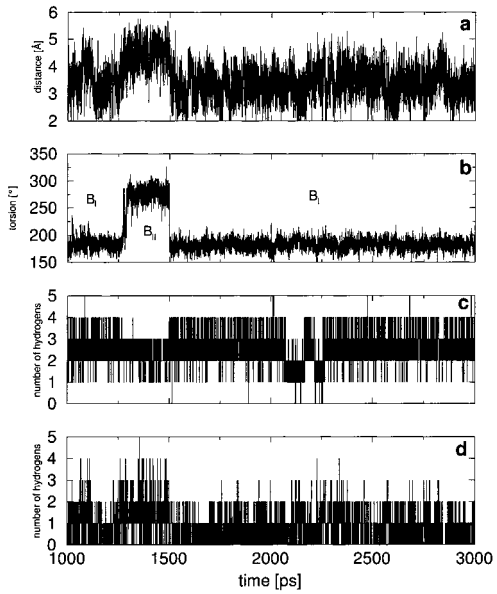


**Figure 7.** Substate interconversion of the G4−A5 base step: The destacking reference C1′−C1′ distance[36] between two adjacent base pairs is monitored as a function of time in the top part (a). In (b) the development of the corresponding $\epsilon$ backbone angle is shown. The two bottom parts (c) and (d) represent the hydration of the phosphate oxygen (c) by the number of water hydrogens closer than 2.2 Å and the hydration of sugar A5 (d) by the number of water hydrogens closer than 3.0 Å, respectively. The reduced hydration in (c) around 2100 and 2200 ps is caused by ion pair formation (see Figure 10).

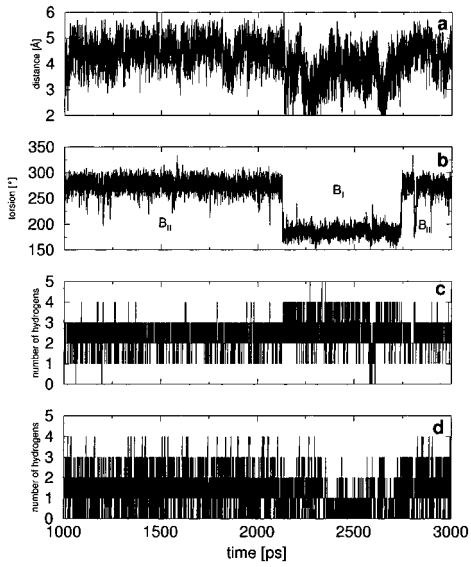


**Figure 8.** Substate interconversion of the G22−C23 base step: The destacking C1′−C1′ distance[36] between two adjacent base pairs is monitored as a function of time in the top picture (a). In (b) the development of the corresponding $\epsilon$-backbone angle is shown. The two bottom pictures (c) and (d) represent the hydration of the phosphate oxygen (c) by the number of water hydrogens closer than 2.2 Å and the hydration of sugar G22 (d) by the number of water hydrogens closer than 3.0 Å, respectively.

exclusively observed in the interconverted $B_{II}$ state (not shown in Figure 6). The latter is in agreement with the X-ray structure of the native dodecamer where the G10−C11 step and the G22−C23 step are found to be in the $B_{II}$ conformation.[23] Comparison with the observed $B_I-B_{II}$ transitions reported by Young et al.[31] is only qualitatively, as they indicate no time scale for the transitions appearing on G2, C23, G4, C9, G10, and T19.

Analysis of the substates of paired bases reveals only one backbone pair, where both phosphate groups are interconverted simultaneously, nevertheless only through a very short period. This C1−G2 C23−G24 base step pair is defined by the $\epsilon$-2 and $\epsilon$-24 angle.

Examination of the possible transition sites, which remain longer in the $B_{II}$ substate, show a preference for pyrimidine−purine steps (5 out of 7). The corresponding pyrimidine−purine steps are the C1−G2, C9−G10, C13−G14, and C15−G16 steps, the corresponding purine−purine step is G4−A5. However, there are also two purine−pyrimidine steps which exhibit significant $B_{II}$ activity. Those steps are G14−C15 and G22−C23.

**3.3. Mechanism of the Substate Interconversion.** The transition between $B_I$ and $B_{II}$ phosphate substates is very fast (i.e., no intermediates are distinguishable on the 0.1 ps time scale). The $\epsilon$-angles for the G4−A5 and G22−C23 steps (which are representative for all investigated steps occuring during the simulation) are shown as a function of time in the middle of Figures 7 and 8. It should be noted that during the time depicted in Figures 7 and 8 the G4−A5 step is predominantly in the $B_I$ state, whereas the G22−C23 step is in the $B_{II}$ conformation. The change from 180° (characterising the $B_I$ state) to 270° ($B_{II}$) is immediate. Taking into account the mechanism suggested by Grzeskowiak et al.[36] we investigated the destacking of adjacent base pairs by using the projected C1′ (sugar carbon attached to the base) distances as criterion ($D_{xy}$). As presented in Figures 7a and 8a, there is indeed a distinct correlation between the destacking of two adjacent base pairs and the $B_I-B_{II}$ transition. This destacking process is much slower and the ring delocation takes some 50 ps until the transition of the backbone conformation occurs. In Figure 7 the destacking process starts at about 1200 ps; the substate interconversion happens some 50 ps later at the climax of destacking. The same is valid for Figure 8, where destacking starts at about 2650 ps resulting in a phosphate switch some 50 ps later. The transition back to the $B_I$ state is accompanied by a fast "restacking". It has been noted that destacking is necessary, but not sufficient for substate interconversion.[36] This is obvious from Figure 8 where two destacking processes take place between 2000 and 2500 ps, but no substate interconversion is observed.

Due to the conformational $B_I-B_{II}$ change, the phosphate atom is shifted toward the minor groove, whereas the phosphate oxygens as well as the phosphodiester oxygens are moved away from it. These movements result in a change of the phosphate's hydration shell in a way that the average number of water molecules around one of the oxygens is decreased. This reduced hydration is visible in Figures 7c and 8c, where the number of water hydrogens nearer than 2.2 Å is plotted as a function of time. The reason for this decreased hydrogen bonding can be easily deduced from Figure 9, where the two substates of the G10−C11 step are shown.

The left-hand picture shows the $B_I$ state where the oxygen on the right side is easily accessible to water. Upon substate transition to $B_{II}$, this oxygen is turned toward the backbone and sterically hinders solvation in comparison to the $B_I$ substate. Analysis of the radial distribution function (rdf) of the hydrogen oxygen distribution reveals that the average number of water hydrogens nearer than 2.5 Å is decreased, whereas the hydration on the other phosphate oxygen as well as on the sugar ring oxygen increases (Figures 7d and 8d).

**3.4. Analysis of the Counterions.** The process of ion pair formation and dissociation was monitored during the simulation. In Figure 10 existing ion pairs are represented by dots/lines as a function of time and a function of the phosphate oxygen number. Comparison with base steps in the $B_{II}$ substate (Figure

**TABLE 2: Analysis of the Nucleic Acid Database[88] with Respect to $B_I-B_{II}$ Conformational Substates and Dependence on X-ray Resolution[a]**

| resolution [Å] | no. of base steps | no. of $B_I$ | percentage $B_I$ | no. of $B_{II}$ | percentage $B_{II}$ | ratio $B_I/B_{II}$ |
|---|---|---|---|---|---|---|
| 3.0 | 5468 | 3727 | 68.2 | 792 | 14.5 | 4.71 |
| 2.5 | 4462 | 3071 | 68.8 | 703 | 15.8 | 4.37 |
| 2.0 | 1684 | 1158 | 68.8 | 321 | 19.1 | 3.61 |
| 1.9 | 1056 | 718 | 68.0 | 240 | 22.7 | 2.99 |
| 1.8 | 650 | 409 | 62.9 | 191 | 29.4 | 2.14 |
| 1.6 | 283 | 193 | 68.2 | 73 | 25.8 | 2.64 |
| 1.4 | 94 | 65 | 69.2 | 27 | 28.7 | 2.41 |

[a] A useful comparison is only valid for structures with a resolution of less than 2.0 Å because above this resolution too many base steps appear in an undefined B-form.

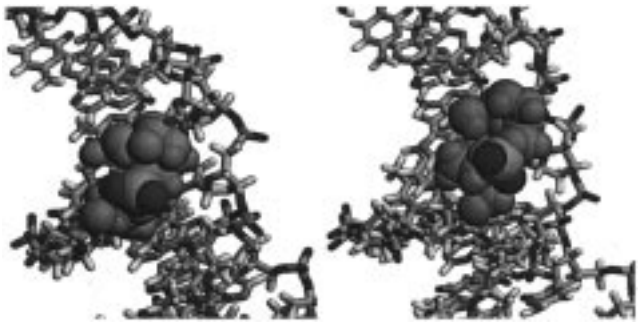

**Figure 9.** $B_I$ (left) and $B_{II}$ (right) substates of the G10−C11 step. The DNA backbone is represented by sticks, whereas the nearest atoms to the phosphate group are shown as spheres. The phosphate oxygen atoms of C11 are colored dark. This representation was created using RasMol 2.6.[91]

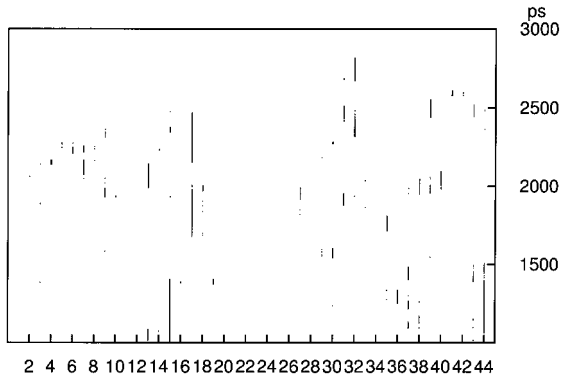


**Figure 10.** Ion pair formation as a function of time: The time during which a sodium counterion forms an ion pair, with one of the phosphate oxygens is marked by a black line/dot. The *x*-axis represents the number of the phosphate oxygen which is involved in the ion pair (i.e., O1 and O2 on P2, O3 and O4 on P3, O23 and O24 on P14).

6) reveals no direct correlation between these two processes. Analysis of the number of ion pairs and the number of phosphates in the $B_I$ substate (Figure 3) with respect to a mutual correlation supports this finding as there is obviously no relation between the number of ion pairs and the number of flipped $\epsilon$-angles. The effect of ion pair formation on the hydration shell is also seen in Figures 7 and 8. The reduced hydration of the G4−A5 step between 2100 and 2300 results from ion pair formation seen in Figure 10 with oxygen number 7; the reduced hydration of the G22−C23 step is seen around 2600 ps on oxygen number 41.

## 4. Discussion

In contrast to X-ray structures of single crystals, the simulation reveals the interconversion of many base steps. As there are only two $B_{II}$ base steps in the X-ray structure, but 15 base steps undergoing substate interconversion in the simulation, it is obvious that in the static X-ray structure only a minor fraction of the allowed interconversions are frozen in. It is important to note that the G10−C11 base step seen in X-ray single crystal studies in the $B_{II}$ substate is observable in our MD simulation as $B_{II}$ mainly between 300 to 1000 ps, whereas from 1000 to 3000 ps this base step is only momentarily in the $B_{II}$ substate around 1800 ps (see Figure 6). Since the system is probably not fully equilibrated between 300 and 1000 ps, our observations of the G10−C11 base step in the $B_{II}$ conformation could be caused by nonequilibrium. If this is true, on crystallization of the dodecamer, $B_{II}$ conformer substates could be sampled which are not those characterized in the equilibrated aqueous solution. Therefore, biologically relevant conclusions of $B_I-B_{II}$ occupation from single-crystal studies could be misleading.

The biologically active B-form in solution is thus in a constant process of substate interconversion. To investigate the $B_I/B_{II}$ ratio in the MD simulation with respect to all known B-DNA structures in the Nucleic Acid Database (NDB),[88] an analysis of all deposited 143 B-DNA double helices was carried out (Tables 2 and 3). To distinguish between the substates, modified rules derived from Schneider et al.[35] were applied. The $B_I$ substate was characterized by $120° < \epsilon < 210°$ and $210° < \zeta < 295°$; the $B_{II}$ conformation by $210° < \epsilon < 300°$ and $150° < \zeta < 210°$. Table 2 shows that a useful comparison is only valid for structures with a resolution of less than 2.0 Å. Above this resolution too many base steps appear in an undefined B-form. This 2.0 Å resolution limit was already shown by Hartmann and Lavery[89] for reliable sugar pucker values. The resulting $B_I/B_{II}$ ratio is between 2 and 3 in comparison to an average of 9.1 in the simulation. However, at a given time the $B_I/B_{II}$ ratio can be as low as 2.7 during the simulation. A further MD simulation with reduced water content (i.e., with $\Gamma = 13$) suggests increasing $B_{II}$ population with decreasing hydration level.

To investigate any sequence preferences for B-substate interconversion (as suggested by Grzeskowiak et al.[36]) another analysis of the NDB was carried out and related to the results obtained from our simulation. For this purpose the base steps of all deposited structures with a resolution lower than 2.0 Å were investigated and their substate determined (Table 3). The results clearly demonstrate a $B_I-B_{II}$ transition preference for pyrimidine−purine (Y−R) steps in comparison to purine−purine (R−R) and purine−pyrimidine (R−Y) steps. The interconversion of pyrimidine−pyrimidine (Y−Y) steps is obviously disfavored. This is in agreement with results from our simulation, where Y−R step transitions (five out of seven) dominate, two R−Y steps exhibit significant $B_{II}$ activity, and no Y−Y step is found to interconvert. This analysis extends the rules derived by Grzeskowiak et al.[36] from four decamer structures. They suggested that $B_{II}$ interconversion is only allowed at Y−R and R−R steps, but never at Y−Y or R−Y steps.

**TABLE 3: Analysis of the Nucleic Acid Database[88] with Respect to the Sequence Dependence of $B_I-B_{II}$ Conformational Substates[a]**

| base step | number of steps | number of steps in $B_{II}$ | percentage $B_{II}$ |
|---|---|---|---|
| AA | 111 | 8 | 7.2 |
| AC | 22 | 0 | 0.0 |
| AG | 52 | 5 | 9.6 |
| AT | 153 | 1 | 0.7 |
| CA | 78 | 61 | 78.2 |
| CC | 85 | 10 | 11.8 |
| CG | 345 | 49 | 14.2 |
| CT | 49 | 0 | 0.0 |
| GA | 111 | 17 | 15.3 |
| GC | 191 | 55 | 28.8 |
| GG | 87 | 39 | 44.8 |
| GT | 15 | 0 | 0.0 |
| TA | 50 | 18 | 36.0 |
| TC | 106 | 0 | 0.0 |
| TG | 77 | 49 | 63.6 |
| TT | 113 | 0 | 0.0 |
| $\Sigma$ | 1645 | 312 | 19.0 |
| R−R | 361 | 69 | 19.1 |
| R−Y | 381 | 56 | 14.7 |
| Y−R | 550 | 177 | 32.2 |
| Y−Y | 353 | 10 | 2.8 |

[a] Only the usual DNA-bases adenine (A), cytosine (C), guanine (G), and thymine (T) were used, the 39 inosine (I) base involving steps were omitted. A summary with respect to pyrimidine (Y) and purine (R) bases is found at the bottom of the table and reveals a preference for pyrimidine−purine (Y−R) steps in comparison to purine-purine (R−R) and purine−pyrimidine (R−Y) steps. The interconversion of pyrimidine−pyrimidine (Y−Y) steps is obviously disfavored.

The mechanism proposed by Grzeskowiak et al.[36] assumes destacking of base pairs followed by $B_I-B_{II}$ substate interconversion. This is consistent with the results of our simulation. The simulation allows for the first time the investigation of the time scale of these two processes and their correlation. In addition, a new process involved in the substate interconversion, the change of the hydration shell, is revealed. This change in the hydrogen-bonding pattern of the phosphate oxygen supposedly leads to an increase of the P−O bond strength and thus to an increase of the frequency of the $PO_2^-$ stretching vibrations. The investigation of B substate dynamics in hydrated B-DNA from salmon testes by Rüdisser et al.[32] showed upon substate interconversion pronounced changes in the $PO_2^-$ stretching band region. These spectroscopic changes are consistent with $B_I$ to $B_{II}$ substate interconversion, considering the changes in hydration shell observed in our MD simulation (see Figures 7 and 8).

## 5. Summary and Conclusions

A state-of-the-art molecular dynamics simulation has been carried out for a period of 3 ns using the *Eco*RI DNA dodecamer as target. The analysis with respect to the $B_I$ and $B_{II}$ conformational substates (characterized by different backbone conformations) revealed a highly dynamical system. Fifteen out of the 22 base steps exhibit $B_I-B_{II}$ transitions, although the average occupation of the $B_{II}$ state is only about 10%. Examination of the transition mechanism resulted in a two step model: Slow buildup of base destacking leads to a very fast $B_I-B_{II}$ switch of the corresponding base step's conformation. This conformational change is accompanied by a reduction of the hydration shell of one of the phosphate oxygens. This mechanism closely matches recently reported spectroscopic features of B-DNA substate dynamics. Comparison of the obtained sequence dependent transition patterns with experimentally determined B-DNA double helices deposited in the Nucleic Acid Database are consistent with our results.

**6. Acknowledgment.** We are grateful for financial support by the Austrian Science Foundation (Project No. P12319-PHY).

## References and Notes

(1) Chang, K.-Y.; Varani, G. *Nature Struct. Biol.* **1997**, *NMR supplement*, 854−858.
(2) Szyperski, T.; Fernandez, C.; Ono, A.; Kainosho, M.; Wüthrich, K. *J. Am. Chem. Soc.* **1998**, *120*, 821−822.
(3) Mitra, R.; Petitt, B. M.; Blake, R. D. *Biopolymers* **1995**, *36*, 169−179.
(4) Berman, H. M. *Curr. Opin. Struct. Biol.* **1994**, *4*, 345−350.
(5) Neidle, S. *Biopolymers (Nucleic Acid Sci.)* **1997**, *44*, 105−121.
(6) Phillips, S. E. V.; Moras, D. *Curr. Opin. Struct. Biol.* **1993**, *3*, 1−2.
(7) Suzuki, M.; Yagi, N. *J. Mol. Biol.* **1996**, *255*, 677−687.
(8) Thuong, N. T.; Hélène, C. *Angew. Chem., Int. Ed.* **1993**, *32*, 666−690.
(9) Suck, D.; Lahm, A.; Oefner, C. *Nature* **1988**, *332*, 464−468.
(10) Otwinowski, Z.; Schevitz, R. W.; Zhang, R. G.; Lawson, C. L.; Joachimiak, A.; Marmorstein, R. Q.; Luisi, B. F.; Sigler, P. B. *Nature* **1988**, *335*, 321−329.
(11) Wolberger, C.; Dong, Y. C.; Ptashne, M.; Harrison, S. C. *Nature* **1988**, *335*, 789−795.
(12) Jordan, S. R.; Pabo, C. O. *Science* **1988**, *242*, 893−899.
(13) Carrondo, M. A.; Coll, M.; Aymami, J.; Wang, A. H.; van der Marel, G. A.; van Boom, J. H.; Rich, A. *Biochemistry* **1989**, *28*, 7849−7859.
(14) Luisi, B. F.; Xu, W. X.; Otwinowski, Z.; Freedman, L. P.; Yamamoto, K. R.; Sigler, P. B. *Nature* **1991**, *352*, 497−505.
(15) Somers, W. S.; Phillips, S. E. V. *Nature* **1992**, *359*, 387−393.
(16) Beamer, L. J.; Pabo, C. O. *J. Mol. Biol.* **1992**, *227*, 177−196.
(17) Beese, L. S.; Derbyshire, V.; Steitz, T. A. *Science* **1993**, *260*, 352−355.
(18) Shakked, Z.; Guzikevich-Guerstein, G.; Frolow, F.; Rabinovich, D.; Joachimiak, A.; Sigler, P. B. *Nature* **1994**, *368*, 469−473.
(19) Luger, K.; Mäder, A. W.; Richmond, R. K.; Sargent, D. F.; Richmond, T. J. *Nature* **1997**, *389*, 251−260.
(20) Rhodes, D. *Nature* **1997**, *389*, 231−233.
(21) Chen, Y.-Q.; Gosh, S.; Gosh, G. *Nature Struct. Biol.* **1998**, *5*, 67−73.
(22) Gupta, G.; Bansal, M.; Sasiskharan, V. *Proc. Natl. Acad. Sci. U.S.A.* **1980**, *77*, 6486−6490.
(23) Fratini, A. V.; Kopka, M. L.; Drew, H. R.; Dickerson, R. E. *J. Biol. Chem.* **1982**, *257*, 14686−14707.
(24) Privé, G. P.; Heinemann, U.; Chandrasegaran, S.; Kan, L.-S.; Kopka, M. L.; Dickerson, R. E. *Science* **1987**, *238*, 498−504.
(25) Shindo, H.; Fujiwara, T.; Akutsu, H.; Masumoto, U.; Shimidzu, M. *J. Mol. Biol.* **1984**, *174*, 221−229.
(26) Sklenar, V.; Bax, A. *J. Am. Chem. Soc.* **1987**, *109*, 7525−7526.
(27) Gorenstein, D. G. *Methods Enzymol.* **1992**, *211*, 254−286.
(28) Gorenstein, D. G. *Chem. Rev.* **1994**, *94*, 1315−1338.
(29) Hartmann, B.; Piazzola, D.; Lavery, R. *Nucleic Acids Res.* **1993**, *21*, 561−568.
(30) Cheatham, T. E., III; Kollman, P. A. *J. Am. Chem. Soc.* **1997**, *119*, 4805−4825.
(31) Young, M. A.; Ravishanker, G.; Beveridge, D. L. *Biophys. J.* **1997**, *73*, 2313−2336.
(32) Rüdisser, S.; Hallbrucker, A.; Mayer, E. *J. Am. Chem. Soc.* **1997**, *119*, 12251−12256.
(33) Szyperski, T.; Ono, A.; Fernandez, C.; Iwai, H.; Tate, S.; Wüthrich, K.; Kainosho, M. *J. Am. Chem. Soc.* **1997**, *119*, 9901−9902.
(34) Berman, H. M. *Biopolymers* **1997**, *44*, 23−44.
(35) Schneider, B.; Neidle, S.; Berman, H. M. *Biopolymers* **1997**, *42*, 113−124.
(36) Grzeskowiak, K.; Yanagi, K.; Privé, G. G.; Dickerson, R. E. *J. Biol. Chem.* **1991**, *266*, 8861−8883.
(37) Cruse, W. B. T.; Salisbury, S. A.; Brown, T.; Cosstick, R.; Eckstein, F.; Kennard, O. *J. Mol. Biol.* **1986**, *192*, 891−905.
(38) Kennard, O.; Hunter, W. N. *Angew. Chem., Int. Ed.* **1991**, *30*, 1254−1277.
(39) Drew, H. R.; Samson, S.; Dickerson, R. E. *Proc. Natl. Acad. Sci. U.S.A.* **1982**, *79*, 4040−4044.
(40) Wing, R.; Drew, H.; Takano, T.; Broka, C.; Tanaka, S.; Itakura, K.; Dickerson, R. E. *Nature* **1980**, *287*, 755−758.
(41) Drew, H. R.; Wing, R. M.; Takanao, T.; Broka, C.; Tanaka, S.; Itakura, K.; Dickerson, R. E. *Proc. Natl. Acad. Sci. U.S.A.* **1981**, *78*, 2179−2183.
(42) Dickerson, R. E.; Drew, H. R. *J. Mol. Biol.* **1981**, *149*, 761−786.
(43) Drew, H. R.; Dickerson, R. E. *J. Mol. Biol.* **1981**, *151*, 535−556.

(44) Dickerson, R. E.; Drew, H. R. *Proc. Natl. Acad. Sci. U.S.A.* **1981**, *78*, 7318−7322.
(45) Kopka, M. L.; Fratini, A. V.; Drew, H. R.; Dickerson, R. E. *J. Mol. Biol.* **1983**, *163*, 129−146.
(46) Westhof, E. *J. Biomol. Struct. Dyn.* **1987**, *5*, 581−600.
(47) Shui, X.; McFail-Isom, L.; Hu, G. G.; Williams, L. D. *Biochemistry* **1998**, *37*, 8341−8355.
(48) Lane, A.; Jenkins, T. C.; Brown, T.; Neidle, S. *Biochemistry* **1991**, *30*, 1372−1385.
(49) Whitka, J. M.; Swaminathan, S.; Srinivasan, J.; Beveridge, D. L.; Bolton, P. H. *Science* **1992**, *255*, 597−599.
(50) Denisov, V. P.; Carlstöm, G.; Venu, K.; Halle, B. *J. Mol. Biol.* **1997**, *268*, 118−136.
(51) Weidlich, T.; Lindsay, S. M.; Rui, Q.; Rupprecht, A.; Peticolas, W. L.; Thomas, G. A. *J. Biomol. Struct. Dyn.* **1990**, *8*, 139−171.
(52) Ravishanker, G.; Swaminathan, S.; Beveridge, D. L.; Lavery, R.; Sklenar, H. *J. Biomol. Struct. Dyn.* **1989**, *6*, 669−699.
(53) Srinivasan, J.; Withka, J. M.; Beveridge, D. L. *Biophys. J.* **1990**, *58*, 533−547.
(54) Prevost, C.; Louise-May, S.; Ravishanker, G.; Lavery, R.; Beveridge, D. L. *Biopolymers* **1993**, *33*, 335−350.
(55) Swaminathan, S.; Ravishanker, G.; Beveridge, D. L. *J. Am. Chem. Soc.* **1991**, *113*, 5027−5040.
(56) Miaskiewicz, K.; Osman, R.; Weinstein, H. *J. Am. Chem. Soc.* **1993**, *115*, 1526−1537.
(57) Duan, Y.; Wilkosz, P.; Rosenberg, J. M. *J. Mol. Biol.* **1996**, *264*, 546−555.
(58) Monaco, R. R.; Polkosnik, W.; Dwarakanath, S. *J. Biomol. Struct. Dyn.* **1997**, *15*, 63−67.
(59) Young, M. A.; Jayaram, B.; Beveridge, D. L. *J. Am. Chem. Soc.* **1997**, *119*, 59−69.
(60) Duan, Y.; Wilkosz, P.; Crowley, M.; Rosenberg, J. M. *J. Mol. Biol.* **1997**, *272*, 553−572.
(61) Cieplak, P.; Cheatham, T. E., III; Kollman, P. A. *J. Am. Chem. Soc.* **1997**, *119*, 6722−6730.
(62) Grable, J.; Frederick, C. A.; Samudzi, C.; Jacobson, L. J.; Lesser, D.; Greene, P.; Boyer, H. W.; Itakura, K.; Rosenberg, J. M. *J. Biomol. Struct. Dyn.* **1984**, *1*, 1149−1160.
(63) Kim, Y.; Grable, J. C.; Love, R.; Greene, P.; Rosenberg, J. M. *Science* **1990**, *249*, 1307−1309.
(64) Wang, Y.; Thomas, G. A.; Peticolas, W. *J. Biomol. Struct. Dyn.* **1987**, *5*, 249−274.
(65) Dickerson, R. E.; Goodsell, D. S.; Kopka, M. L.; Pjura, P. E. *J. Biomol. Struct. Dyn.* **1987**, *5*, 557−579.
(66) Jain, S.; Sundaraligam, M. *J. Mol. Biol.* **1989**, *264*, 12780−12784.
(67) Heinemann, U.; Hahn, M. *J. Biol. Chem.* **1992**, *267*, 7332−7341.
(68) von Kitzing, E. *Methods Enzymol.* **1992**, *211*, 449−467.
(69) Beveridge, D. L.; Swaminathan, S.; Ravishanker, G.; Withka, J. M.; Srinivasan, J.; Prevost, C.; Louise-May, S.; Langley, D. R.; DiCapua, F. M.; Bolton, P. H. Molecular Dynamics Simulations on the Hydration, Structure and Motions of DNA Oligomers. In *Water and Biological Molecules*; The Macmillan Press Ltd.: London, 1993; pp 165−225.
(70) Beveridge, D. L.; Ravishanker, G. *Curr. Opin. Struct. Biol.* **1994**, *4*, 246−255.
(71) Louise-May, S.; Auffinger, P.; Westhof, E. *Curr. Opin. Struct. Biol.* **1996**, *6*, 289−298.
(72) Hogan, M. E.; Jardetzky, O. *Proc. Natl. Acad. Sci. U.S.A.* **1979**, *76*, 6341−6345.
(73) Roongta, V. A.; Jones, C. R.; Gorenstein, D. G. *Biochemistry* **1990**, *29*, 5245−5258.
(74) Pearlman, D. A.; Case, D. A.; Caldwell, J. W.; Ross, W. S.; Cheatham, T., III; Ferguson, D. M.; Seibel, G. L.; Singh, U. C.; Weiner, P. K.; Kollman, P. A. *AMBER 4.1*; University of California: San Francisco, 1995.
(75) York, D. M.; Wlodawer, A.; Pedersen, L. G.; Darden, T. A. *Proc. Natl. Acad. Sci. U.S.A.* **1994**, *91*, 8715−8718.
(76) Cheatham, T. E., III; Miller, J. L.; Fox, T.; Darden, T. A.; Kollman, P. A. *J. Am. Chem. Soc.* **1995**, *117*, 4193−4194.
(77) Young, M. A.; Nirmala, R.; Srinivasan, J.; McConnell, K. J.; Ravishanker, G.; Beveridge, D. L.; Berman, H. M. Analysis of helix bending in crystal structures and molecular dynamics simulations of DNA oligonucleotides. In *Structural Biology: The State of the Art*; Adenine Press: Albany, NY, 1994; pp 197−214.
(78) Cheatham, T. E., III; Kollman, P. A. *J. Mol. Biol.* **1996**, *259*, 434−444.
(79) Sen, S.; Nilsson, L. *J. Am. Chem. Soc.* **1998**, *120*, 619−631.
(80) Luo, J.; Bruice, T. C. *J. Am. Chem. Soc.* **1998**, *120*, 1115−1123.
(81) de Souza, O. N.; Ornstein, R. L. *J. Biomol. Struct. Dyn.* **1997**, *14*, 607−611.
(82) de Souza, O. N.; Ornstein, R. L. *Biophys. J.* **1997**, *72*, 2395−2397.
(83) Arnott, S.; Campbell-Smith, P. J.; Chandrasekaran, R. Atomic coordinates and molecular conformation for DNA-DNA, RNA-RNA, and DNA-RNA helices. In *CRC Handbook of Biochemistry and Molecular Biology*; CCRC Press: Boca Raton, 1976; pp 411−422.
(84) Chandrasekaran, R.; Arnott, S. *J. Biomol. Struct. Dyn.* **1996**, *13*, 1015−1027.
(85) Jorgensen, W. L. *J. Am. Chem. Soc.* **1981**, *103*, 335−340.
(86) Cornell, W. D.; Cieplak, P.; Bayly, C. I.; Goult, I. R.; Merz, K. M., Jr.; Ferguson, D. M.; Spellmeyer, D. C.; Fox, T.; Caldwell, J. W.; Kollman, P. A. *J. Am. Chem. Soc.* **1995**, *117*, 5179−5197.
(87) Berendsen, H. J. C.; Postma, J. P. M.; van Gunsteren, W. F.; DiNola, A.; Haak, J. R. *J. Chem. Phys.* **1984**, *81*, 3684−3690.
(88) Berman, H. M.; Olson, W. K.; Beveridge, D. L.; Westbrook, J.; Gelbin, A.; Demeny, T.; Hsieh, S.-H.; Srinivasan, A. R.; Schneider, B. *Biophys. J.* **1992**, *63*, 751−759.
(89) Hartmann, B.; Lavery, R. *Quart. Rev. Biophys.* **1996**, *29*, 309−368.
(90) Schaftenaar, G. *MOLDEN 3.2*; University of Nijmegen: The Netherlands, 1991.
(91) Sayle, R. *RasMol 2.6*; Glaxo Wellcome Medicines Research Centre: Hertfordshire, U.K., 1995.